# Calculation of predictions for non-identical particle correlations in heavy ions collisions at LHC energies from hydrodynamics-inspired models

MASTER OF SCIENCE THESIS

Author:
**Mateusz Wojciech Gałażyn**

Supervisor:
**Prof. Adam Kisiel**

Warsaw, 18th September 2014

# Wyznaczenie przewidywań teoretycznych dla korelacji cząstek nieidentycznych w zderzeniach ciężkich jonów przy energiach LHC w modelach opartych na hydrodynamice

PRACA MAGISTERSKA


Autor:
**Mateusz Wojciech Gałażyn**

Promotor:
**dr hab. inż. Adam Kisiel, prof. PW**


Warszawa, 18 września 2014

# Abstract

# Streszczenie

# Contents

# Introduction

# Chapter 1

# Theory of heavy ion collisions

## 1.1 The Standard Model

In the 1970s, a new theory of fundamental particles and their interaction emerged. A new concept, which concerns the electromagnetic, weak and strong nuclear interactions between know particles. This theory is called *The Standard Model*. There are seventeen named particles in the standard model, organized into the chart shown below (Fig. 1.1). Fundamental particles are divided into two families: *fermions* and *bosons*.

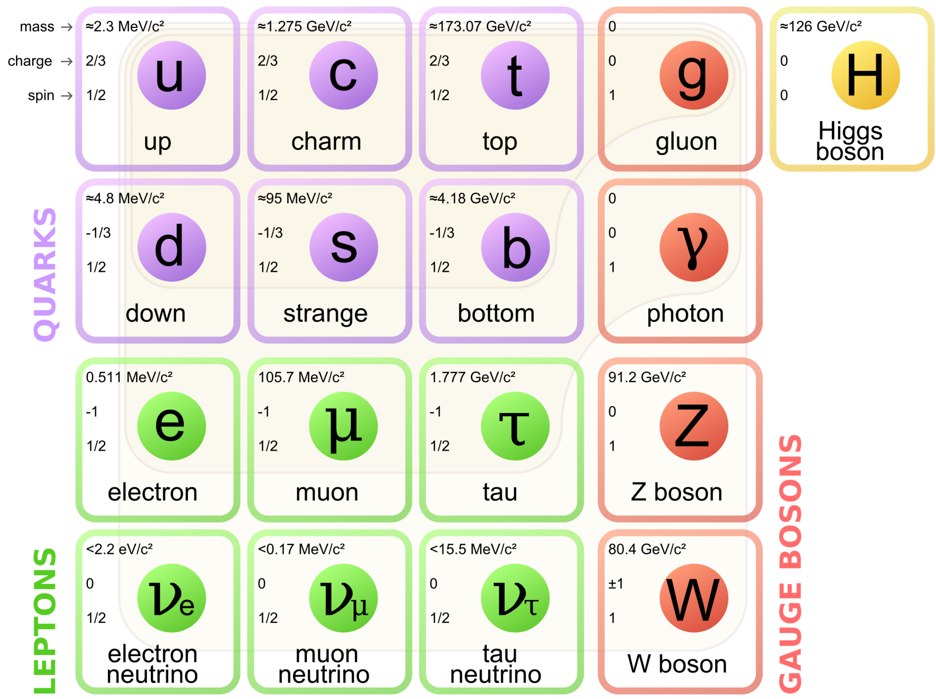


Figure 1.1: The Standard Model of elementary particles [1].

Fermions are the building blocks of matter. They are divided into two groups. Six of them, which must bind together are called *quarks*. Quarks are known to bind into doublets (*mesons*), triplets (*baryons*) and recently confirmed four-quark states.[1] Two of baryons, with the longest lifetimes, are forming a nucleus: a proton and a neutron. A proton is build from two up quarks and one down, and neutron consists of two down quarks and one up. A proton is found to be a stable particle (at least it has a lifetime larger than $10^{35}$ years) and a free neutron has a mean lifetime about $8.8 \times 10^2$ s. Fermions, that can exist independently are called *leptons*. Neutrinos are a subgroup of leptons, which are only influenced by weak interaction. Fermions can be divided into three generations (three columns in the Figure 1.1). Generation I particles can combine into hadrons with the longest life spans. Generation II and III consists of unstable particles which form also unstable hadrons.

Bosons are force carriers. There are four fundamental forces: weak - responsible for radioactive decay, strong - coupling quarks into hadrons, electromagnetic - between charged particles and gravity - the weakest, which causes the attraction between particles with a mass. The Standard Model describes the first three. The weak force is mediated by $W^{\pm}$ and $Z^0$ bosons, electromagnetic force is carried by photons $\gamma$ and the carriers of a strong interaction are gluons *g*. The fifth boson is a Higgs boson which is responsible for giving other particles mass.

## 1.2 Quantum Chromodynamics

### 1.2.1 Quarks and gluons

Quarks interact with each other through the strong interaction. The mediator of this force is a *gluon* - a massless and chargeless particle. In the quantum chromodynamics (QCD) - theory describing strong interaction - there are six types of "charges" (like electrical charges in the electrodynamics) called *colours*. The colours were introduced because some of the observed particles, like $\Delta^-$, $\Delta^{++}$ and $\Omega^-$ appeared to consist of three quarks with the same flavour (*ddd*, *uuu* and *sss* respectively), which was in conflict with the Pauli principle. One quark can carry one of the three colours (usually called *red*, *green* and *blue*) and antiquark one of the three anti-colours respectively. Only colour-neutral (or white) particles could exist. Mesons are assumed to be a colour-anticolour pair, while baryons are *red-green-blue* triplets. Gluons also are colour-charged and there are 8 types of gluons. Therefore they can interact with themselves [3].

[1] The LHCb experiment at CERN in Geneva confirmed recently existence of $Z(4430)$ - a particle consisting of four quarks [2].

### 1.2.2 Quantum Chromodynamics potential

As a result of that gluons are massless, one can expect, that the static potential in the QCD will have the similar form like one in the electrodynamics e.g. $\sim 1/r$ (through an analogy to photons). In reality the QCD potential is assumed to have the form of [3]

$$V_s = -\frac{4}{3}\frac{\alpha_s}{r} + kr \,, \tag{1.1}$$

where the $\alpha_s$ is a coupling constant of the strong force and the $kr$ part is related with the *confinement*. In comparison to the electromagnetic force, a value of the strong coupling constant is $\alpha_s \approx 1$ and the electromagnetic one is $\alpha = 1/137$.

The fact that quarks does not exist separately, but they are always bound, is called a confinement. As two quarks are pulled apart, the linear part $kr$ in the Eq. 1.1 becomes dominant and the potential becomes proportional to the distance. This situation resembles stretching of a string. At some point, when the string is so large it is energetically favourable to create a quark-antiquark pair. At this moment such pair (or pairs) is formed, the string breaks and the confinement is preserved (Fig. 1.2).

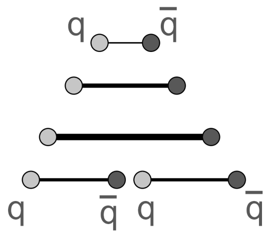


Figure 1.2: A string break and a creation of a pair quark-anti-quark [4].

On the other hand, for the small $r$, an interaction between the quarks and gluons is dominated by the Coulomb-like term $-\frac{4}{3}\frac{\alpha_s}{r}$. The coupling constant $\alpha_s$ depends on the four-momentum $Q^2$ transferred in the interaction. This dependence is presented in Fig. 1.3. The value $\alpha_s$ decreases with increasing momentum transfer and the interaction becomes weak for large $Q^2$, i.e. $\alpha_s(Q) \to 0$. Because of weakening of coupling constant, quarks at large energies (or small distances) are starting to behave like free particles. This phenomenon is known as an *asymptotic freedom*. The QCD potential has also temperature dependence - the force strength "melts" with the temperature increase. Therefore the asymptotic freedom is expected to appear in either the case of high baryon densities (small distances between quarks) or very high temperatures. This temperature dependence is illustrated in the Fig. 1.4.

If the coupling constant $\alpha_s$ is small, one can use perturbative methods to calculate physical observables. Perturbative QCD (pQCD) successfully describes hard processes (with large $Q^2$), such as jet production in high energy proton-antiproton collisions. The applicability of pQCD is defined by the *scale parameter*

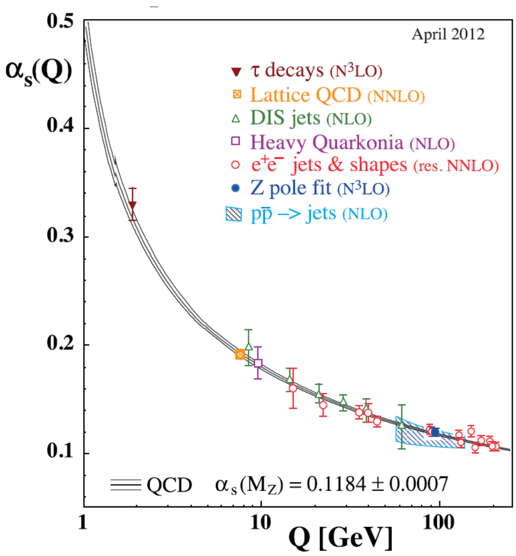


Figure 1.3: The coupling parameter $\alpha_s$ dependence on four-momentum transfer $Q^2$ [5].

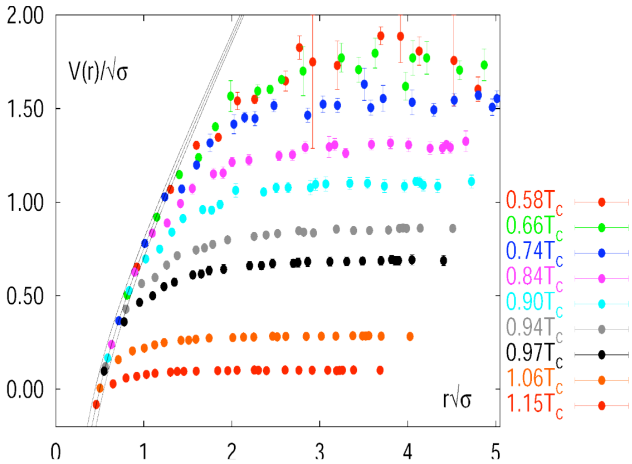


Figure 1.4: The QCD potential for a pair quark-antiquark as a function of distance for different temperatures. A value of a potential decreases with the temperature [4].

$\Lambda_{QCD} \approx 200$ MeV. If $Q \gg \Lambda_{QCD}$ then the process is in the perturbative domain and can be described by pQCD. A description of soft processes (when $Q < 1$ GeV) is a problem in QCD - perturbative theory breaks down at this scale. Therefore, to describe processes with low $Q^2$, one has to use alternative methods like Lattice QCD. Lattice QCD (LQCD) is non-perturbative implementation of a field theory in which QCD quantities are calculated on a discrete space-time grid. LQCD allows to obtain properties of matter in equilibrium, but there are some limitations. Lattice QCD requires fine lattice spacing to obtain precise results - therefore large computational resources are necessary. With the constant growth of computing power this problem will become less important. The second problem is that lattice simulations are possible only for baryon density $\mu_B = 0$. At $\mu_B \neq 0$, Lattice QCD breaks down because of the sign problem [6].

### 1.2.3 The quark-gluon plasma

The new state of matter in which quarks are no longer confined is known as a *quark-gluon plasma* (QGP). The predictions coming from the discrete space-time Lattice QCD calculations reveal a phase transition from the hadronic matter to the quark-gluon plasma at the high temperatures and baryon densities. The res-

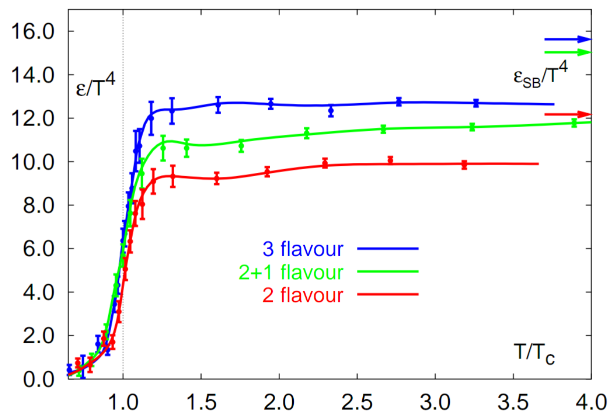


Figure 1.5: A number of degrees of freedom as a function of a temperature [7].

ults obtained from such calculations are shown on Fig. 1.5. The energy density $\epsilon$ which is divided by $T^4$ is a measure of number of degrees of freedom in the system. One can observe significant rise of this value, when the temperature increases past the critical value $T_C$. Such increase is signaling a phase transition - the formation of QGP [8]. The values of the energy densities plotted in Fig. 1.5 do not reach the Stefan-Boltzmann limit $\epsilon_{SB}$ (marked with arrows), which corresponds to an ideal gas. This can indicate some residual interactions in the system. According to the results from the RHIC[2], the new phase of matter behaves more like an ideal fluid, than like a gas [9].

One of the key questions, to which current heavy ion physics tries to find an answer is the value of a critical temperature $T_C$ as a function of a baryon chemical potential $\mu_B$ (baryon density), where the phase transition occur. The results coming from the Lattice QCD are presented in the Fig. 1.6. The phase of matter in which quarks and gluons are deconfined is expected to exist at large

[2] Relativistic Heavy Ion Collider at Brookhaven National Laboratory in Upton, New York

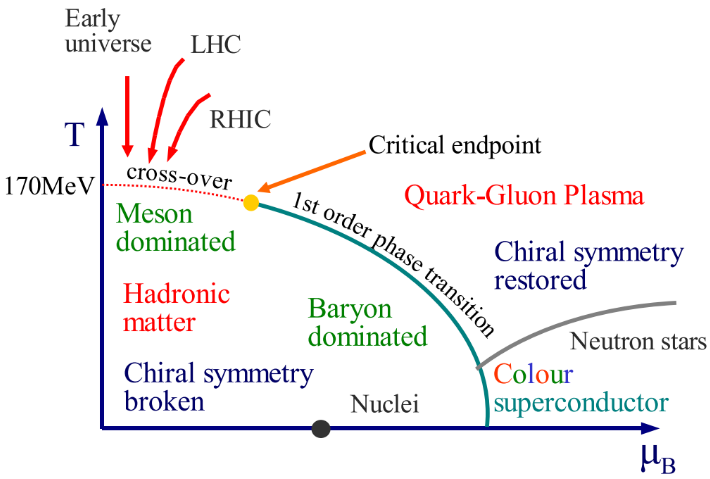


Figure 1.6: Phase diagram coming from the Lattice QCD calculations [8].

temperatures. In the region of small temperatures and high baryon densities, a different state is supposed to appear - a *colour superconductor*. The phase transition between hadronic matter and QGP is thought to be of 1$^{\text{st}}$ order at $\mu_B \gg 0$. However as $\mu_B \to 0$ quarks' masses become significant and a sharp transition transforms into a rapid but smooth cross-over. It is believed that in Pb-Pb collisions observed at the LHC[3], the created matter has high enough temperature to be in the quark-gluon plasma phase, then cools down and converts into hadrons, undergoing a smooth transition [8].

## 1.3 Relativistic heavy ion collisions

### 1.3.1 Stages of heavy ion collision

To create the quark-gluon plasma one has to achieve high enough temperatures and baryon densities. Such conditions can be recreated in the heavy ion collisions at the high energies. The left side of the Figure 1.7 shows simplified picture of a central collision of two highly relativistic nuclei in the centre-of-mass reference frame. The colliding nuclei are presented as thin disks because of the Lorentz contraction. In the central region, where the energy density is the highest, a new state of matter - the quark-gluon plasma - is supposedly created. Afterwards, the plasma expands ad cools down, quarks combine into hadrons and their mutual interactions cease when the system reaches the *freeze-out* temperature. Subsequently, produced free hadrons move towards the detectors.

On the right side of the Figure 1.7 there is presented a space-time evolution of a collision process, plotted in the light-cone variables (z, t). The two highly

[3] Large Hadron Collider at CERN, Geneva

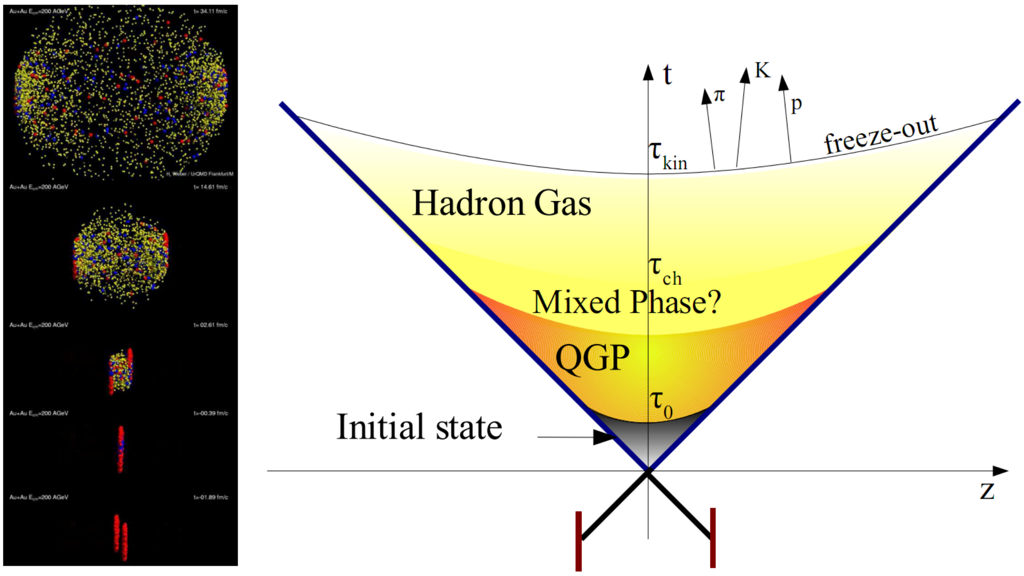


Figure 1.7: Left: stages of a heavy ion collision simulated in the UrQMD model. Right: schematic view of a heavy ion collision evolution [8].

relativistic nuclei are traveling basically along the light cone until they collide at the centre of diagram. Nuclear fragments emerge from the collision again along the (forward) light cone, while the matter between fragmentation zones populates the central region. This hot and dense matter is believed to be in the state of the quark-gluon plasma. There exist several frameworks to describe this transition to the QGP phase, for example: QCD string breaking, QCD parton cascades or colour glass condensate evolving into glasma and later into quark-gluon plasma [10].

**String breaking** – In the string picture, the nuclei pass through each other forming colour strings. This is analogous to the situation depicted in the Fig 1.2 - the colour string is created between quarks inside particular nucleons in nuclei. In the next step strings decay / fragment forming quarks and gluons or directly hadrons. This approach becomes invalid at very high energies, when the strings overlap and cannot be treated as independent objects.

**Parton cascade** – The parton[4] cascade model is based on the pQCD. The colliding nuclei are treated as clouds of quarks and which penetrate through each other. The key element of this method is the time evolution of the partion phase-space distributions, which is governed by a relativistic Boltzmann equation with a collision term that contains dominant perturbative QCD interations. The bottleneck of the parton cascade model is the low energies regime, where the $Q^2$ is too small to be described by the perturbative theory.

[4] A parton is a common name for a quark and a gluon.

**Colour glass condensate –** The colour glass condensate assumes, that the hadron can be viewed as a tightly packed system of interacting gluons. The saturation of gluons increases with energy, hence the total number of gluons may increase without the bound. Such a saturated and weakly coupled gluon system is called a colour glass condensate. The fast gluons in the condensate are Lorentz contracted and redistributed on the two very thin sheets representing two colliding nuclei. The sheets are perpendicular to the beam axis. The fast gluons produce mutually orthogonal colour magnetic and electric fields, that only exist on the sheets. Immediately after the collision, i.e. just after the passage of the two gluonic sheets after each other, the longitudinal electric and magnetic fields are produced forming the *glasma*. The glasma fields decay through the classical rearrangement of the fields into radiation of gluons. Also decays due to the quantum pair creations are possible. In this way, the quark-gluon plasma is produced.

Interactions within the created quark-gluon plasma bring the system into the local statistical equilibrium, hence its further evolution can be described by the relativistic hydrodynamics. The hydrodynamic expansion causes that the system becomes more and more dilute. The phase transition from the quark-gluon plasma to the hadronic gas occurs. Further expansion causes a transition from the strongly interaction hadronic gas to weakly interacting system of hadrons which move freely to the detectors. Such decoupling of hadrons is called the *freeze-out*. The freeze-out can be divided into two phases: the chemical freeze-out and the thermal one. The *chemical freeze-out* occurs when the inelastic collisions between constituents of the hadron gas stop. As the system evolves from the chemical freeze-out to the thermal freeze-out the dominant processes are elastic collisions (such as, for example $\pi + \pi \to \rho \to \pi + \pi$) and strong decays of heavier resonances which populate the yield of stable hadrons. The *thermal freeze-out* is the stage of the evolution of matter, when the strongly coupled system transforms to a weakly coupled one (consisting of essentially free particles). In other words this is the moment, where the hadrons practically stop to interact. Obviously, the temperatures corresponding to the two freeze-outs satisfy the condition

$$T_{chem} > T_{therm} \; , \tag{1.2}$$

where $T_{chem}$ (inferred from the ratios of hadron multiplicities) is the temperature of the chemical freeze-out, and $T_{therm}$ (obtained from the investigation of the transverse-momentum spectra) is the temperature of the thermal freeze-out [10].

### 1.3.2 QGP signatures

The quark-gluon plasma is a very short living and unstable state of matter. One cannot investigate the properties of a plasma and confirm its existence directly. Hence, the several experimental effects were proposed as QGP signatures, some of them have been already observed in heavy ion experiments [8]. As matter created in the heavy ions collisions is supposed to behave like a fluid, one should expect appearance of collective behaviour at small transverse momenta - so called *elliptic flow* and *radial flow*. The next signal is the temperature range obtained from the measurements of *direct photons*, which gives us information, that the system created in heavy ion collisions is far above the critical temperature obtained from the LQCD calculations. The *puzzle in the di-lepton spectrum* can be explained by the modification of spectral shape of vector mesons (mostly $\rho$ meson) in the presence of a dense medium. This presence of a medium can also shed light on the *jet quenching* phenomenon - the suppression occurence in the high $p_T$ domain.

### Elliptic flow

In a non-central heavy ion collisions, created region of matter has an almond shape with its shorter axis in the *reaction plane* (Fig. 1.8). The pressure gradient is much larger in-plane rather than out-of-plane. This causes larger acceleration and transverse velocities in-plane rather than out-of-plane. Such differences can

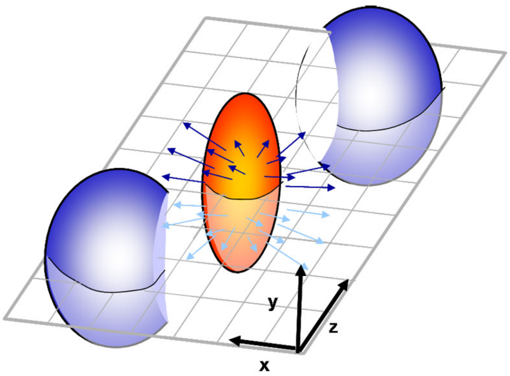


Figure 1.8: Overlapping region which is created in heavy ion collisions has an almond shape. Visible x-z plane is a *reaction plane*. The x-y plane is a *transverse plane*. The z is a direction of the beam [11].

be investigated by studying the distribution of particles with respect to the reaction plane orientation [12]:

$$E\frac{d^3N}{dp^3} = \frac{1}{2\pi}\frac{d^2N}{p_T dp_T dy}(1 + 2v_1\cos(\phi) + 2v_2\cos(2\phi) + ...)\ , \tag{1.3}$$

where $\phi$ is the angle between particle transverse momentum $p_T$ (a momentum projection on a transverse plane) and the reaction plane, $N$ is a number of particles and $E$ is an energy of a particle. The $y$ variable is a *rapidity* defined as:

$$y = \frac{1}{2}\ln\left(\frac{E+p_L}{E-p_L}\right)\ , \tag{1.4}$$

where $p_L$ is a longitudinal component of a momentum (paralel to the beam direction). The $v_n$ coefficients indicate the shape of a system. For the most central collisions (b = 0 - see Fig. 1.9) all coefficients vanish $\bigwedge_{n \in N_+} v_n = 0$ (the overlapping region has the spherical shape). The Fourier series elements in the parentheses

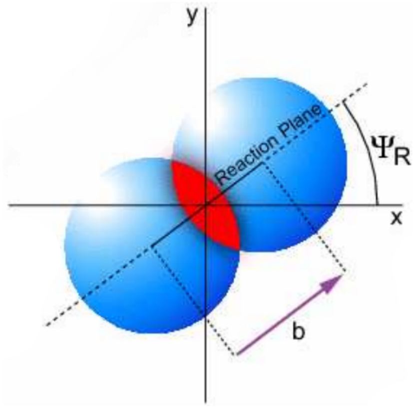


Figure 1.9: Cross-section of a heavy ion collision in a transverse plane. $\Psi_R$ is an angle between transverse plane and the reaction plane. The *b* parameter is an *impact parameter* - a distance between centers of nuclei during a collision. An impact parameter is related with the centrality of a collision and a volume of the quark-gluon plasma [12].

in Eq. 1.3 represent different kinds of a flow. The first value: "1" represents the *radial flow* - an isotropic flow in every direction. Next coefficient $v_1$ is responsible for *direct flow*. The $v_2$ coefficient is a measure of elliptic anisotropy (*elliptic flow*). The $v_2$ has to build up in the early stage of a collision - later the system becomes too dilute: space asymmetry and the pressure gradient vanish. Therefore the observation of elliptic flow means that the created matter was in fact a strongly interacting matter.

The $v_2$ coefficient was measured already at CERN SPS, LHC and RHIC. For the first time hydrodynamics successfully described the collision dynamics as the measured $v_2$ reached hydrodynamic limit (Fig. 1.10). As expected, there is a mass ordering of $v_2$ as a function of $p_T$ (lower plot in the Fig. 1.10) with pions having the largest and protons the smallest anisotropy. In the upper plots in the Fig. 1.10 there is a $v_2$ as a function of transverse kinetic energy. The left plot shows the two unversal trend lines for baryons and mesons. After the scaling of $v_2$ and the kinetic energy by the number of valence quarks, all of the hadrons follow the same universal curve. Those plots show that strong collectivity is observed in heavy ion collisions.

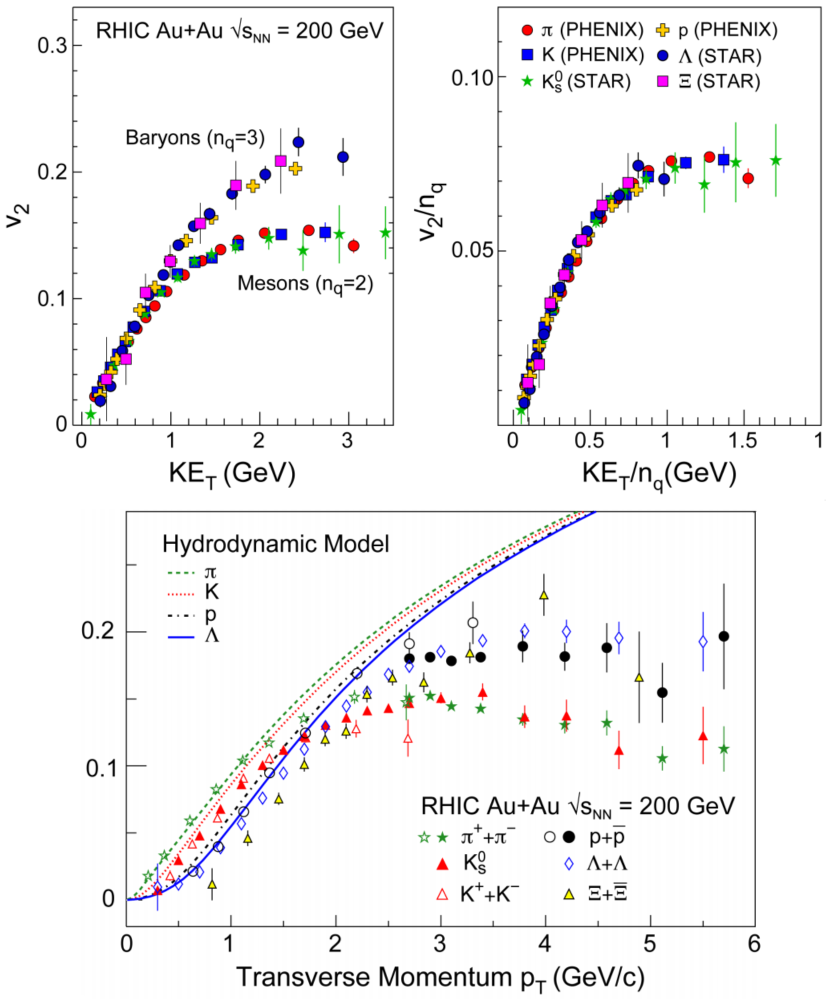


Figure 1.10: *Lower:* The elliptic flow $v_2$ follows the hydrodynamical predictions for an ideal fluid perfectly. Note that $> 99\%$ of all final hadrons have $p_T < 1.5$ GeV/c. *Upper left:* The $v_2$ plotted versus transverse kinetic energy $KE_T = m_T - m_0 = \sqrt{p_T^2 + m_0^2} - m_0$. The $v_2$ follows different universal curves for mesons and baryons. *Upper right:* When scaled by the number of valence quarks, the $v_2$ follows the same universal curve for all hadrons and for all values of scaled transverse kinetic energy [13].

### Transverse radial flow

Elliptic flow described previously is caused by the pressure gradients which must also produce a more simple collective behaviour of matter - a movement inside-out, called radial flow. Particles are pushed to higher momenta and they move away from the center of the collision. A source not showing collective behaviour, like pp collisions, produces particle spectra that can be fitted by a power-law [8]:

$$\frac{1}{2\pi p_T}\frac{d^2N}{dp_T d\eta} = C\left(1+\frac{p_T}{p_0}\right) . \tag{1.5}$$

The $\eta$ variable is a *pseudorapidity* defined as follows:

$$\eta = \frac{1}{2}\ln\left(\frac{p+p_L}{p-p_L}\right) = -\ln\left(\frac{\theta}{2}\right) , \tag{1.6}$$

where $\theta$ is an emission angle $\cos\theta = p_L/p$ .

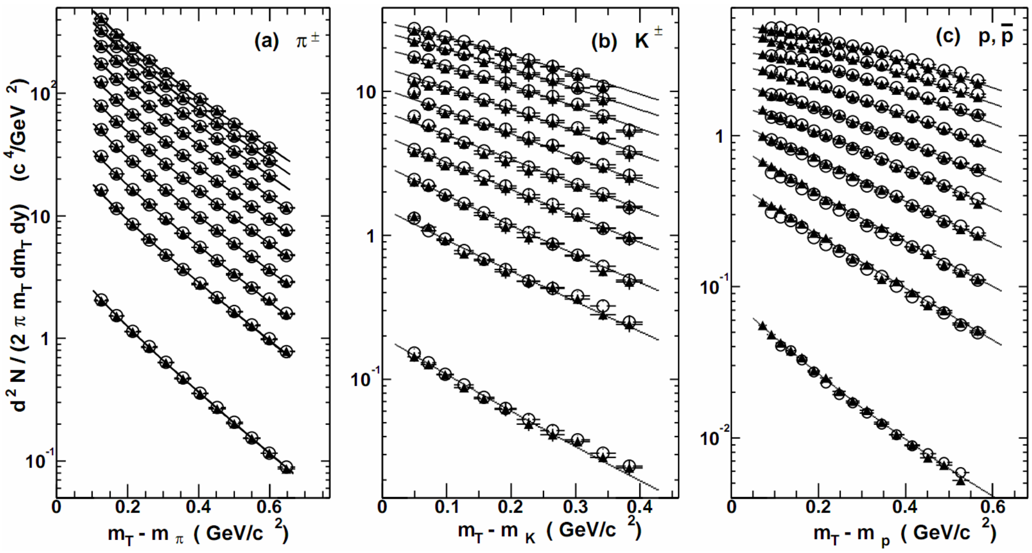


Figure 1.11: Invariant yield of particles versus transverse mass $m_T = \sqrt{p_T^2 + m_0^2}$ for $\pi^{\pm}$, $K^{\pm}$, $p$ and $\bar{p}$ at mid-rapidity for p+p collisions (bottom) and Au+Au events from 70-80% (second bottom) to 0-5% (top) centrality [14].

The hydrodynamical expansion of a system gives the same flow velocity kick for different kind of particles - ones with bigger masses will gain larger $p_T$ boost. This causes increase of the yield of particles with larger transverse momenta. In the invariant yield plots one can observe the decrease of the slope parameter, especially for the heavier hadrons. This is presented in the Fig. 1.11. The most affected spectra are ones of kaons (b) and protons (c). One can notice decrease of the slope parameter for heavy ion collisions (plots from second bottom to top) comparing to the proton-proton collisions (bottom ones), where no boost from radial flow should occur [8].

### Direct photons

The direct photons are photons, which are not coming from the final state hadrons decays. Their sources can be various interaction from charged particles created in the collision, either at the partonic or at the hadronic level. Direct photons are considered to be an excellent probe of the early stage of the collision. This is because their mean free path is very large to the created system in the collision. Thus photons created at the early stage leave the system without suffering any interaction and retain information about this stage, in particular about its temperature.

One can distinguish two kinds of direct photons: *thermal* and *prompt*. Thermal photons can be emitted from the strong processes in the quark-gluon plasma involving quarks and gluons or hot hadronic matter (e.g. processes: $\pi\pi \to \rho\gamma$, $\pi\rho \to \pi\gamma$). Thermal photons can be observed in the low $p_T$ region. Prompt photons are believed to come from "hard" collisions of initial state partons belonging to the colliding nuclei. The prompt photons can be described using the pQCD. They will dominate the high $p_T$ region. The analysis of transverse momentum of spectra of direct photons revealed, that the temperature of the source of thermal photons produced in heavy ion collisions at RHIC is in the range 300-600 MeV (Fig. 1.12). Hence the direct photons had to come from a system whose temperature is far above from the critical temperature for QGP creation.

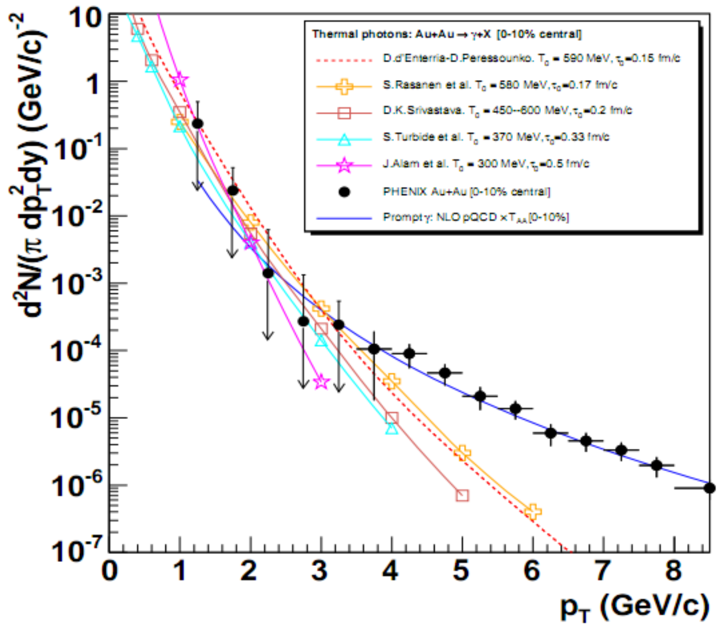


Figure 1.12: Thermal photons spectra for the central Au+Au collisions at $\sqrt{s_{NN}}$ = 200 GeV at computed within different hydrodynamical models compared with the pQCD calculations (solid line) and experimental data from PHENIX (black dots) [15].

### Puzzle in di-lepton mass spectrum

The invariant mass spectra (Fig. 1.13) of lepton pairs reveal many peaks corresponding to direct decays of various mesons into a lepton pair. The continuous background in this plot is caused by the decays of hadrons into more than two leptons (including so-called *Dalitz decays* into a lepton pair and a photon). Particular hadron decay channels, which contribute to this spectrum are shown

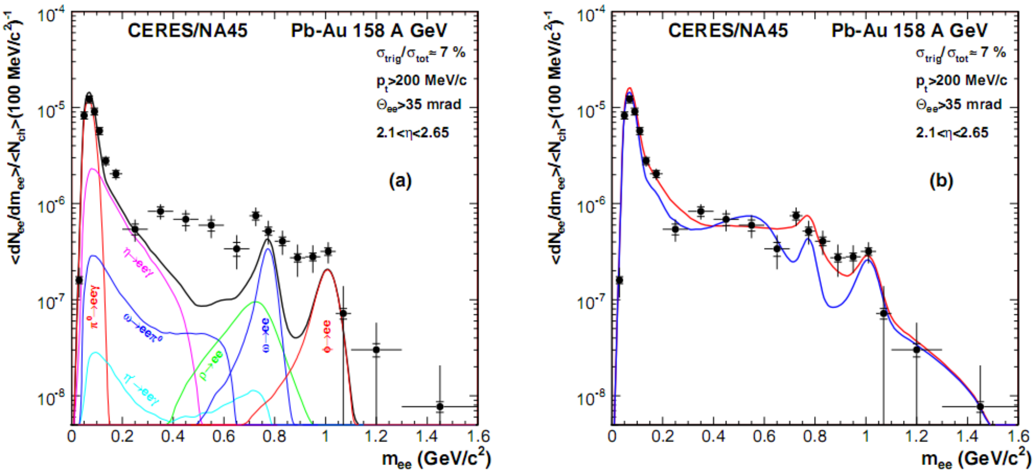


Figure 1.13: Left: Invariant mass spectrum of $e^+$-$e^-$ pairs in Pb+Au collisions at 158$A$ GeV compared to the sum coming from the hadron decays predictions. Right: The expectations coming from model calculations assuming a dropping of the $\rho$ mass (blue) or a spread of the $\rho$ width in the medium (red) [16].

in the Fig. 1.13 with the coloured lines and their sum with the black one. The sum (called *the hadronic cocktail*) of various components describes experimental spectra coming from the simple collisions (like p+p or p+A) quite well with the statistical and systematical uncertainties [9]. This situation is different considering more complicated systems i.e. A+A. Spectra coming from Pb+Au collisions are presented on the plots in the Fig. 1.13. The "hadronic cocktail" does not describe the data, in the mass range between the $\pi$ and the $\rho$ mesons a significant excess of electron pairs over the calculated sum is observed. Theoretical explanation of this phenomenon assumes modification of the spectral shape of vector mesons in a dense medium. Two different interpretations of this increase were proposed: a decrease of meson mass with the medium density and increase of the meson width in the dense medium. In principle, one could think of simultaneous occurrence of both effects: mass shift and resonance broadening. Experimental results coming from the CERES disfavour the mass shift hypothesis indicating only broadening of resonance peaks (Fig. 1.13b) [9].

### Jet quenching

A jet is defined as a group of particles with close vector momenta and high energies. It has its beginning when the two partons are going in opposite directions and have energy big enough to produce new quark-antiquark pair and then radiate gluons. This process can be repeated many times and it results in two back-to-back jets of hadrons. It has been found that jets in the opposite hemisphere (*away-side jets*) show a very different pattern in d+Au and Au+Au collisions. This is shown in the azimuthal correlations in the Fig. 1.14. In d+Au collisions, like in p+p, a pronounced away-side jet appears around $\Delta\phi = \pi$, exactly opposite to the trigger jet, what is typical for di-jet events. In central Au+Au collisions the away jet is suppressed. When the jet has its beginning near the surface of the quark-

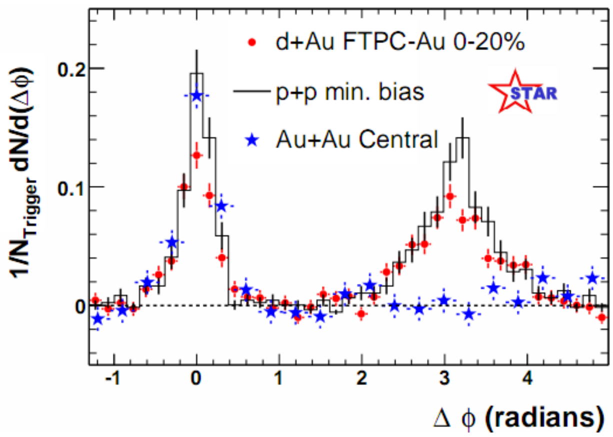


Figure 1.14: Azimuthal angle difference $\Delta\phi$ distributions for different colliding systems at $\sqrt{s_{NN}}$ = 200 GeV. Transverse momentum cut: $p_T > 2$ GeV. For the Au+Au collisions the away-side jet is missing [17].

qluon plasma, one of the jets (*near-side jet*) leaves the system almost without any interactions. This jet is visible on the correlation plot as a high peak at $\Delta\phi = 0$. However, the jet moving towards the opposite direction has to penetrate a dense medium. The interaction with the plasma causes energy dissipation of particles and is visible on an azimuthal correlation plot as disappearance of the away-side jet [9].

# Chapter 2

# Therminator model

`THERMINATOR` [18] is a Monte Carlo event generator designed to investigate the particle production in the relativistic heavy ion collisions. The functionality of the code includes a generation of the stable particles and unstable resonances at the chosen hypersurface model. It performs the statistical hadronization which is followed by space-time evolution of particles and the decay of resonances. The key element of this method is an inclusion of a complete list of hadronic resonances, which contribute very significantly to the observables. The second version of `THERMINATOR` [19] comes with a posibility to incorporate any shape of freeze-out hypersurface and the expansion velocity field, especially those generated externally with various hydrodynamic codes.

## 2.1 (3+1)-dimensional viscous hydrodynamics

Most of the relativistic viscous hydrodynamic calculations are done in (2+1)-dimensions. Such simplification assumes boost-invariance of a matter created in a collision. Experimental data reveals that no boost-invariant region is formed in the collisions [20]. Hence, for the better description of created system a (3+1)-dimensional model is required.

In the four dimensional relativistic dynamics one can describe a system using a space-time four-vector $x^\nu = (ct, x, y, z)$, a velocity four-vector $u^\nu = \gamma(c, v_x, v_y, v_z)$ and a energy-momentum tensor $T^{\mu\nu}$. The particular components of $T^{\mu\nu}$ have a following meaning:

- $T^{00}$ - an energy density,
- $cT^{0\alpha}$ - an energy flux across a surface $x^\alpha$,
- $T^{\alpha 0}$ - an $\alpha$-momentum flux across a surface $x^\alpha$ multiplied by $c$,
- $T^{\alpha\beta}$ - components of momentum flux density tensor,

where $\gamma = (1 - v^2/c^2)^{-1/2}$ is Lorentz factor and $\alpha, \beta \in \{1, 2, 3\}$. Using $u^\nu$ one can express $T^{\mu\nu}$ as follows [21]:

$$T_0^{\mu\nu} = (e + p)u^\mu u^\nu - pg^{\mu\nu} \tag{2.1}$$

where $e$ is an energy density, $p$ is a pressure and $g^{\mu\nu}$ is an inverse metric tensor:

$$g^{\mu\nu} = \begin{bmatrix} 1 & 0 & 0 & 0 \\ 0 & -1 & 0 & 0 \\ 0 & 0 & -1 & 0 \\ 0 & 0 & 0 & -1 \end{bmatrix}. \tag{2.2}$$

The presented version of energy-momentum tensor (Eq. 2.1) can be used to describe dynamics of a perfect fluid. To take into account influence of viscosity, one has to apply the following corrections coming from shear $\pi^{\mu\nu}$ and bulk $\Pi$ viscosities [22]:

$$T^{\mu\nu} = T_0^{\mu\nu} + \pi^{\mu\nu} + \Pi(g^{\mu\nu} - u^\mu u^\nu). \tag{2.3}$$

The stress tensor $\pi^{\mu\nu}$ and the bulk viscosity $\Pi$ are solutions of dynamical equations in the second order viscous hydrodynamic framework [21]. The comparison of hydrodynamics calculations with the experimental results reveal, that the shear viscosity divided by entropy $\eta/s$ has to be small and close to the AdS/CFT estimate $\eta/s$ = 0.08 [22, 23]. The bulk viscosity over entropy value used in calculations is $\zeta/s$ = 0.04 [22].

When using $T^{\mu\nu}$ to describe system evolving close to local thermodynamic equilibrium, relativistic hydrodynamic equations in a form of:

$$\partial_\mu T^{\mu\nu} = 0 \tag{2.4}$$

can be used to describe the dynamics of the local energy density, pressure and flow velocity.

Hydrodynamic calculations are starting from the Glauber [1] model initial conditions. The collective expansion of a fluid ends at the freeze-out hypersurface. That surface is usually defined as a constant temperature surface, or equivalently as a cut-off in local energy density. The freeze-out is assumed to occur at the temperature $T$ = 140 MeV.

## 2.2 Statistical hadronization

Statistical description of heavy ion collision has been successfully used to describe quantitatively *soft* physics, i.e. the regime with the transverse momentum not exceeding 2 GeV. The basic assumption of the statistical approach of evolution of the quark-gluon plasma is that at some point of the

[1]The Glauber Model is used to calculate "geometrical" parameters of a collision like an impact parameter, number of participating nucleons or number of binary collisions.

space-time evolution of the fireball, the thermal equilibrium is reached. When the system is in the thermal equilibrium the local phase-space densities of particles follow the Fermi-Dirac or Bose-Einstein statistical distributions. At the end of the plasma expansion, the freeze-out occurs. The freeze-out model incorporated in the `THERMINATOR` model assumes, that chemical and thermal freeze-out occur at the same time.

### 2.2.1 Cooper-Frye formalism

The result of the hydrodynamic calculations is the freeze-out hypersurface $\Sigma^\mu$. A three-dimensional element of the surface is defined as [19]

$$d\Sigma_\mu = \epsilon_{\mu\alpha\beta\gamma}\frac{\partial x^\alpha}{\partial\alpha}\frac{\partial x^\beta}{\partial\beta}\frac{\partial x^\gamma}{\partial\gamma}d\alpha d\beta d\gamma, \tag{2.5}$$

where $\epsilon_{\mu\alpha\beta\gamma}$ is the Levi-Civita tensor and the variables $\alpha, \beta, \gamma \in \{1, 2, 3\}$ are used to parametrize the three-dimensional freeze-out hypersurface in the Minkowski four-dimensional space. The Levi-Civita tensor is equal to 1 when the indices form an even permutation (eg. $\epsilon_{0123}$), to -1 when the permutation is odd (e.g. $\epsilon_{2134}$) and has a value of 0 if any index is repeated. Therefore [19],

$$d\Sigma_0 = \begin{vmatrix} \frac{\partial x}{\partial\alpha} & \frac{\partial x}{\partial\beta} & \frac{\partial x}{\partial\gamma} \\ \frac{\partial y}{\partial\alpha} & \frac{\partial y}{\partial\beta} & \frac{\partial y}{\partial\gamma} \\ \frac{\partial z}{\partial\alpha} & \frac{\partial z}{\partial\beta} & \frac{\partial z}{\partial\gamma} \end{vmatrix} d\alpha d\beta d\gamma \tag{2.6}$$

and the remaining components are obtained by cyclic permutations of $t$, $x$, $y$ and $z$.

One can obtain the number of hadrons produced on the hypersurface $\Sigma^\mu$ from the Cooper-Frye formalism. The following integral yields the total number of created particles [19]:

$$N = (2s+1)\int\frac{d^3p}{(2\pi)^3E_p}\int d\Sigma_\mu p^\mu f(p_\mu u^\mu)\ , \tag{2.7}$$

where $f(p_\mu u^\mu)$ is the phase-space distribution of particles (for stable ones and resonances). One can simply derive from Eq. 2.7, the dependence of the momentum density [24]:

$$E\frac{d^3N}{dp^3} = \int d\Sigma_\mu f(p_\mu u^\mu)p^\mu\ . \tag{2.8}$$

The momentum distribution $f$ contains non-equilibrium corrections:

$$f = f_0 + \delta f_{shear} + \delta f_{bulk}\ , \tag{2.9}$$

where

$$f_0(p_\mu u^\mu) = \left\{\exp\left[\frac{p_\mu u^\mu - (B\mu_B + I_3\mu_{I_3} + S\mu_S + C\mu_C)}{T}\right] \pm 1\right\}^{-1} \tag{2.10}$$

In case of fermions, in the Eq. 2.10 there is a plus sign and for bosons, minus sign respectively. The thermodynamic quantities appearing in the $f_0(\cdot)$ are $T$ - temperature, $\mu_B$ - baryon chemical potential, $\mu_{I_3}$ - isospin chemical potential, $\mu_S$ - strange chemical potential, $\mu_C$ - charmed chemical potential and the $s$ is a spin of a particle. The hydrodynamic calculations yield the flow velocity at freeze-out as well as the stress and bulk viscosity tensors required to calculate non-equilibrium corrections to the momentum distribution used in Eq. 2.7. The term coming from shear viscosity has a form [22]

$$\delta f_{shear} = f_0(1 \pm f_0)\frac{1}{2T^2(e+p)}p^\mu p^\nu \pi_{\mu\nu} \tag{2.11}$$

and bulk viscosity

$$\delta f_{bulk} = C f_0(1 \pm f_0)\left(\frac{(u^\mu p_\mu)^2}{3u^\mu p_\mu} - c_s^2 u^\mu p_\mu\right)\Pi \tag{2.12}$$

where $c_s$ is sound velocity and

$$\frac{1}{C} = \frac{1}{3}\frac{1}{(2\pi)^3}\sum_{hadrons}\int d^3p\frac{m^2}{E}f_0(1 \pm f_0)\left(\frac{p^2}{3E} - c_s^2 E\right) . \tag{2.13}$$

The equations presented above are directly used in the `THERMINATOR` to generate the primordial hadrons (created during freeze-out) with the Monte-Carlo method. Resonances produced in this way, propagate and decay, in cascades if necessary. For every generated particle, its origin point either on a hypersurface or is associated with the point of the decay of the parent particle. This information is kept in the simulation due to its importance for the femtoscopic analysis.

# Chapter 3

# Particle interferometry

Two-particle interferometry (also called *femtoscopy*) gives a possibility to investigate space-time characteristics of the particle-emitting source created in heavy ion collisions. Through the study of particle correlations, their momentum distributions can be used to obtain information about the spatial extent of the created system. Using this method, one can measure sizes of the order of $10^{-15}$ m and time of the order of $10^{-23}$ s.

## 3.1 HBT interferometry

In the 1956 Robert Hanbury Brown and Richard Q. Twiss proposed a method which through analysis of interference between photons allowed to investigate angular dimensions of stars. The most important result from the Hanbury-Brown-Twiss experiments is that two indistinguishable particles can produce an interference effect. There is almost no difference between normal interferometry and HBT method, except that the latter one does not take into account information about phase shift of registered particles. At the beginning this method was used in astronomy for photon interference, but this effect can be used also to measure extent of any emitting source. This method was adapted to heavy ion collisions to investigate dimensions of a system created in those collisions by studying correlations of identical particles [25]. The main difference between HBT method in astronomy and femtoscopy is that the first one is based on space-time HBT correlations and the latter one uses momentum correlations. The momentum correlations yield the space-time picture of the source, whereas the space-time HBT correlations provide the characteristic relative momenta of emitted photons, which gives the angular size of the star without the knowledge of its radius and lifetime [10].

## 3.2 Theoretical approach

Intensity interferometry in heavy ion physics uses similar mathematical formalism as the astronomy HBT measurement. Through the measurement of correlation between particles as a function of their relative momentum one can deduce the average separation between emitting sources.

### 3.2.1 Conventions used

In heavy ion collisions to describe particular directions, components of momentum and location of particles, one uses naming convention called the Bertsch-Pratt coordinate system. This system is presented in the Fig. 3.1. The three dir-

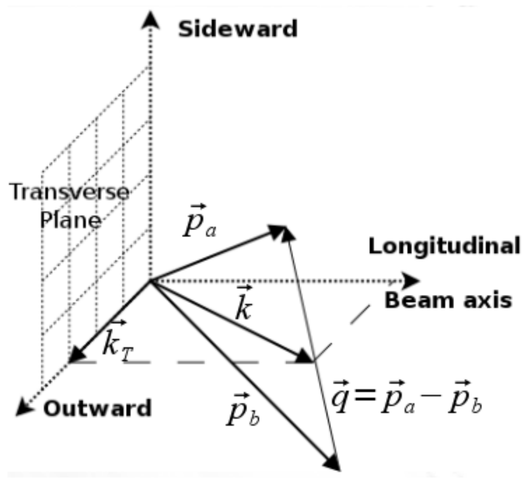


Figure 3.1: Bertsch-Pratt direction naming convention used in heavy ion collision.

ections are called *longitudinal*, *outward* and *sideward*. The longitudinal direction is parallel to the beam axis. The plane perpendicular to the beam axis is called a *transverse plane*. A projection of a particle pair momentum $\mathbf{k} = (\mathbf{p}_a + \mathbf{p}_b)/2$ on a transverse plane (a *transverse momentum* $\mathbf{k}_T$) determines *outward* direction: $(\mathbf{k})_{out} = \mathbf{k}_T$. A direction perpendicular to the longitudinal and outward is called *sideward*.

A particle pair is usually described using two coordinate systems. The first one, *Longitudinally Co-Moving System* (**LCMS**) is moving along the particle pair with the longitudinal direction, in other words, the pair longitudinal momentum vanishes: $(\mathbf{p}_a)_{long} = -(\mathbf{p}_b)_{long}$. The second system is called *Pair Rest Frame* (**PRF**). In the PRF the centre of mass rests: $\mathbf{p}_a = -\mathbf{p}_b$. Variables which are expressed in the PRF are marked with a star (e.g. $\mathbf{k}^*$).

The transition of space-time coordinates from LCMS to PRF is simply a boost along the outward direction, with the transverse velocity of the pair $\beta_t = (\mathbf{v}/c)_{out}$ [25]:

$$\begin{aligned} r^*_{out} &= \gamma_t(r_{out} - \beta_t \Delta t) && (3.1)\\ r^*_{side} &= r_{side} && (3.2)\\ r^*_{long} &= r_{long} && (3.3)\\ \Delta t^* &= \gamma_t(\Delta t - \beta_t r_{out}) \ , && (3.4) \end{aligned}$$

where $\gamma_t = (1-\beta_t^2)^{-1/2}$ is the Lorentz factor. However, in calculations performed in this work the equal time approximation is used, which assumes that particles in a pair were produced at the same time in PRF - the $\Delta t^*$ is neglected.

The most important variables used to describe particle pair are their total momentum $\mathbf{P} = \mathbf{p}_a + \mathbf{p}_b$ and relative momentum $\mathbf{q} = \mathbf{p_a} - \mathbf{p_b}$. In the PRF one has $\mathbf{q} = 2\mathbf{k}^*$, where $\mathbf{k}^*$ is a momentum of the first particle in PRF.

### 3.2.2 Two particle wave function

Let us consider two identical particles with momenta $\mathbf{p_1}$ and $\mathbf{p_2}$ emitted from space points $\mathbf{x_1}$ and $\mathbf{x_2}$. Those emitted particles can be treated as two incoherent waves. If the particles are identical, they are also indistinguishable, therefore one

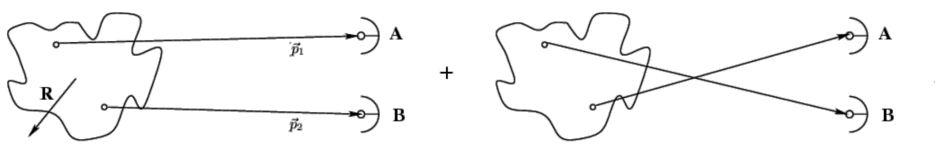


Figure 3.2: The pair wave function is a superposition of all possible states. In case of particle interferometry it includes two cases: particles with momenta $p_1$, $p_2$ registered by detectors *A*, *B* and $p_1$, $p_2$ registered by *B*, *A* respectively.

has also take into account the scenario, where the particle with momentum $\mathbf{p_1}$ is emitted from $\mathbf{x_2}$ and particle $\mathbf{p_2}$ from $\mathbf{x_1}$ (Fig. 3.2). In such case, the wave function describing behaviour of a pair has to contain both components [8]:

$$\Psi_{ab}(\mathbf{q}) = \frac{1}{\sqrt{2}} \left[\exp(-i\mathbf{p_1}\mathbf{x_1} - i\mathbf{p_2}\mathbf{x_2}) \pm \exp(-i\mathbf{p_2}\mathbf{x_1} - i\mathbf{p_1}\mathbf{x_2})\right] \ . \tag{3.5}$$

A two particle wave function of identical bosons is symmetric ("+" sign in Eq. 3.5) and in case of identical fermions - antisymmetric ("-" sign). This anti-symmetrization or symmetrization implies the correlation effect coming from the Fermi-Dirac or Bose-Einstein statistics accordingly.

To provide full description of a system consisting of two charged hadrons, one has to include in the wave function besides quantum statistics also Coulomb and strong Final State Interactions. Considering identical particles systems, the quantum statistics is a main source of a correlation. Hence, in case of space-time analysis of particle emitting source, effects coming from the Coulomb and Strong interactions can be neglected.

### 3.2.3 Source emission function

To describe particle emitting source, one uses a single emission function [25]:

$$S_A(\mathbf{x}_1, \mathbf{p}_1) = \int S(\mathbf{x}_1, \mathbf{p}_1, \mathbf{x}_2, \mathbf{p}_2, ..., \mathbf{x}_N, \mathbf{p}_N) d\mathbf{x}_2 d\mathbf{p}_2 ... d\mathbf{x}_N d\mathbf{p}_N \tag{3.6}$$

and a two-particle one:

$$S_{AB}(\mathbf{x}_1, \mathbf{p}_1, \mathbf{x}_2, \mathbf{p}_2) = \int S(\mathbf{x}_1, \mathbf{p}_1, \mathbf{x}_2, \mathbf{p}_2, ..., \mathbf{x}_N, \mathbf{p}_N) d\mathbf{x}_3 d\mathbf{p}_3 ... d\mathbf{x}_N d\mathbf{p}_N \ . \tag{3.7}$$

Emission function $S(\cdot)$ can be interpreted as a probability to emit a particle, or a pair of particles from a given space-time point with a given momentum. In principle, the source emission function should encode all physics aspects of the particle emission process i.e. the symmetrization for bosons and fermions, as well as the two-body and many body Final State Interactions. Instead of this, one assume that each particle's emission process is independent - the interaction between final-state particles after their creation is independent from their emission process. The assumption of this independence allows to construct two-particle emission function from single particle emission functions via a convolution [25]:

$$\begin{aligned} S(\mathbf{k}^*, \mathbf{r}^*) = \int S_A(\mathbf{p}_1, \mathbf{x}_1) S_B(\mathbf{p}_2, \mathbf{x}_2) \delta \left[ \mathbf{k}^* - \frac{\mathbf{p}_1 + \mathbf{p}_2}{2} \right] \delta \left[ \mathbf{r}^* - (\mathbf{x}_1 + \mathbf{x}_2) \right] \\ \times\, d^4\mathbf{x}_1 d^4\mathbf{x}_2 d^4\mathbf{x}_1 d^3\mathbf{p}_1 d^3\mathbf{p}_2 \end{aligned} \tag{3.8}$$

In case of identical particles, ($S_A = S_B$) several simplifications can be made. A convolution of the two same Gaussian distributions is also a Gaussian distribution with $\sigma$ multiplied by $\sqrt{2}$. Femtoscopy can give information only about two-particle emission function, but when considering Gaussian distribution as a source function in Eq. 3.8, one can obtain a $\sigma$ of a single emission function from a two-particle emission function. The Eq. 3.8 is not reversible - an information about $S_A(\cdot)$ cannot be derived from $S_{AB}(\cdot)$. An exception from this rule is a Gaussian source function, hence it is often used in femtoscopic calculations. Considering pairs of identical particles, an emission function is assumed to be described by the following equation in the Pair Rest Frame [25]:

$$S_{1D}^{PRF}(\mathbf{r}^*) = \exp\left( - \frac{{r^*_{out}}^2 + {r^*_{side}}^2 + {r^*_{long}}^2}{4{R_{inv}}^2} \right) \ . \tag{3.9}$$

To change from the three-dimensional variables to the one-dimensional variable one requires introduction of the proper Jacobian $r^{*2}$:

$$\boxed{S_{1D}^{PRF}(r^*) = r^{*2} \exp\left( - \frac{r^{*2}}{4{R_{inv}}^2} \right)} \ . \tag{3.10}$$

The “4” in the denominator before the “standard deviation” $R_{inv}$ in the Gaussian distribution comes from the convolution of the two Gaussian distributions, which multiplies the $R_{inv}$ by a factor of $\sqrt{2}$.

A more complex form of emission function was used by all RHIC and SPS experiments in identical pion femtoscopy:

$$\boxed{S_{3D}^{LCMS}(\mathbf{r}) = \exp\left(-\frac{r_{out}^2}{4{R_{out}}^2} - \frac{r_{side}^2}{4{R_{side}}^2} - \frac{r_{long}^2}{4{R_{long}}^2}\right)} . \tag{3.11}$$

The main difference of this source function is that it has three different and independent widths $R_{out}$, $R_{side}$, $R_{long}$ and they are defined in the LCMS, not in PRF. Unlike in PRF, in LCMS an equal-time approximation is not used. For identical particles this is not a problem - only Coulomb interaction inside a wave function depends on $\Delta t$.

**Relationship between one-dimensional and three-dimensional source sizes**

Up to now, most of femtoscopic measurements were limited only to averaged source size $R_{av}^L$ (the letter “L” in superscript stands for LCMS):

$$S_{1D}^{LCMS}(\mathbf{r}) = \exp\left(-\frac{{r_{out}}^2 + {r_{side}}^2 + {r_{long}}^2}{2{R_{av}^L}^2}\right) . \tag{3.12}$$

The relationship between between $S_{1D}^{LCMS}(\cdot)$ and $S_{3D}^{LCMS}(\cdot)$ is given by:

$$\begin{aligned} S_{3D}^{LCMS}(r) = \int \exp\left(-\frac{r_{out}^2}{2{R_{out}^L}^2} - \frac{r_{side}^2}{2{R_{side}^L}^2} - \frac{r_{long}^2}{2{R_{long}^L}^2}\right) \\ \times\, \delta\left(r - \sqrt{r_{out}^2 + r_{side}^2 + r_{long}^2}\right) dr_{out} dr_{side} dr_{long} . \end{aligned} \tag{3.13}$$

The one-dimensional source size corresponding to the three-dimensional one can be approximated by the following form:

$$S_{1D}^{LCMS}(r) = r^2 \exp\left(-\frac{r^2}{2{R_{av}^L}^2}\right) . \tag{3.14}$$

The equation above assumes that $R_{out}^L = R_{side}^L = R_{long}^L$ hence $R_{av}^L = R_{out}^L$. If this condition is not satisfied, one can not give explicit mathematical relation between one-dimensional and three-dimensional source sizes. However, for realistic values of $R$ (i.e. for similar values of $R_{out}$, $R_{side}$, $R_{long}$), the $S_{3D}^{LCMS}$ from Eq. 3.13 is not very different from Gaussian distribution and can be well approximated by Eq. 3.13.

A deformation of an averaged source function in case of big differences in $R_{out}$, $R_{side}$, $R_{long}$ is presented in the Fig. 3.3. A three-dimensional Gaussian distribution with varying widths was averaged into one-dimensional function using

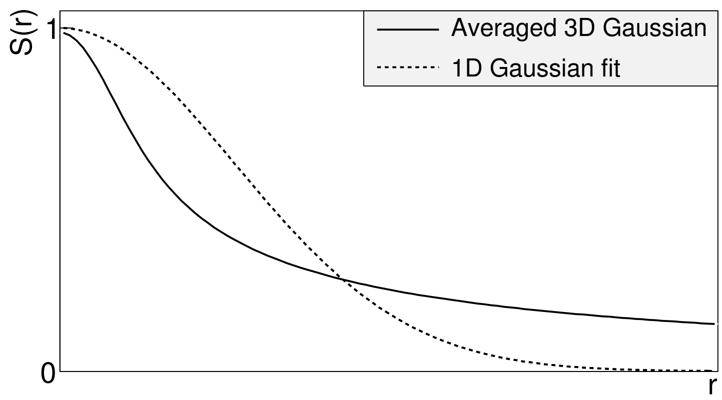


Figure 3.3: An averaged three-dimensional Gaussian source function with different widths was averaged into one-dimensional function. To illustrate deformations, one-dimensional Gaussian distribution was fitted.

the Eq. 3.13. Afterwards, an one-dimensional Gaussian distribution was fitted. One can notice a heavy tail of an averaged distribution in long $r$ region, which makes an approximation using one-dimensional distribution in this case quite inaccurate.

Using Eq. 3.13 and Eq. 3.14 one can obtain a relation between one-dimensional width and the three-dimensional ones. Through numerical calculations one can find the following approximate relation [25]:

$$\boxed{R^L_{av} = \sqrt{\left({R^L_{out}}^2 + {R^L_{side}}^2 + {R^L_{long}}^2\right)\Big/3}\ .} \tag{3.15}$$

This equation does not depend on the pair velocity, hence it is valid in the LCMS and PRF.

### 3.2.4 Theoretical correlation function

The fundamental object in a particle interferometry is a correlation function. The correlation function is defined as:

$$C(\mathbf{p}_a, \mathbf{p}_b) = \frac{P_2(\mathbf{p}_a, \mathbf{p}_b)}{P_1(\mathbf{p}_a)P_1(\mathbf{p}_b)}\ , \tag{3.16}$$

where $P_2$ is a conditional probability to observe a particle with momentum $\mathbf{p}_b$ if particle with momentum $\mathbf{p}_b$ was also observed. A $P_1$ is a probability to observe a particle with a given momentum. The relationship between source emission function, pair wave function and the correlation function is described by the following equation:

$$C(\mathbf{p}_1, \mathbf{p}_2) = \int S_{AB}(\mathbf{p}_1, \mathbf{x}_1, \mathbf{p}_2, \mathbf{x}_2)|\Psi_{AB}|^2 d^4\mathbf{x}_1 d^4\mathbf{x}_2 \tag{3.17}$$

Substituting the one-dimensional emission function (Eq. 3.10) into the integral above yields the following form of correlation function in PRF:

$$\boxed{C(q) = 1 + \lambda \exp\left(-R_{inv}^2 q^2\right)} \tag{3.18}$$

where $q$ is a momentum difference between two particles. When using the three-dimensional emission function (Eq. 3.11) one gets the following correlation function defined in the LCMS:

$$\boxed{C(\mathbf{q}) = 1 + \lambda \exp\left(-R_{out}^2 q_{out}^2 - R_{side}^2 q_{side}^2 - R_{long}^2 q_{long}^2\right)} \tag{3.19}$$

where $q_{out}$, $q_{side}$, $q_{long}$ are $\mathbf{q}$ components in the outward, sideward and longitudinal direction. The $\lambda$ parameter in the equations above determines correlation strength. The lambda parameter has values in the range $\lambda \in [-0.5, 1]$ and it depends on a pair type. In case of pairs of identical bosons (like $\pi$-$\pi$ or $K$-$K$) the lambda parameter $\lambda \to 1$. For identical fermions (e.g. $p$-$p$) $\lambda \to$ -0.5. Values of $\lambda$ observed experimentally are lower than 1 (for bosons) and greater than -0.5 (for fermions). There are few explanations to this effect: detector efficiencies, inclusion of misidentified particles in a used sample or inclusion of non-correlated pairs (when one or both particles come from e.g. long-lived resonance). The analysis carried out in this work uses data from a model, therefore the detector efficiency and particle purity is not taken into account [25].

### 3.2.5 Spherical harmonics decomposition of a correlation function

Results coming from an analysis using three-dimensional correlation function in Cartesian coordinates are quite difficult to visualize. To do that, one usually performs a projection into a one dimension in outward, sideward and longitudinal directions. One may loose important information about a correlation function in this procedure, because it gives only a limited view of the full three-dimensional structure. Recently, a more advanced way of presenting correlation function - a spherical harmonics decomposition, was proposed. The three-dimensional correlation function is decomposed into an infinite set of components in a form of one-dimensional histograms $C_l^m(q)$. In this form, a correlation function is defined as a sum of a series [26]:

$$C(\mathbf{q}) = \sum_{l,m} C_l^m(q) Y_l^m(\theta, \phi) \ , \tag{3.20}$$

where $Y_l^m(\theta, \phi)$ is a spherical harmonic function. Spherical harmonics are an orthogonal set of solutions to the Laplace's equation in spherical coordinates Hence, in this approach, a correlation function is defined as a function of $q$, $\theta$ and $\phi$. To obtain $C_l^m$ coefficients in the series, one has to calculate the following integral:

$$C_l^m(q) = \int_\Omega C(q, \theta, \phi) Y_l^m(\theta, \phi) d\Omega \ , \tag{3.21}$$

where $\Omega$ is a full solid angle.

Spherical harmonics representation has several important advantages. The main advantage of this decomposition is that it requires less statistics than traditional analysis performed in Cartesian coordinates. Another one is that it encodes full three-dimensional information in a set of one-dimensional plots. In principle it does not have to be an advantage, because full description of a correlation function requires infinite number of *l*, *m* components. But it so happens that the intrinsic symmetries of a pair distribution in a femtoscopic analysis result in most of the components to vanish. For the identical particles correlation functions, all coefficients with odd values of *l* and *m* disappear. It has also been shown, that the most significant portion of femtoscopic data is stored in the components with the lowest *l* values. It is expected that, the main femtoscopic information is contained in the following components [25]:

$$C_0^0 \to R_{LCMS} \,, \tag{3.22}$$

$$\Re C_2^0 \to \frac{R_T}{R_{long}} \,, \tag{3.23}$$

$$\Re C_2^2 \to \frac{R_{out}}{R_{side}} \,, \tag{3.24}$$

where $R_{LCMS} = \sqrt{\left({R_{out}}^2 + {R_{side}}^2 + {R_{long}}^2\right)/3}$ and $R_T = \sqrt{\left(R_{out}^2 + R_{side}^2\right)/2}$. The $C_0^0$ is sensitive to the overall size of a correlation function. The $\Re C_2^0$ carries the information about the ratio of the transverse to the longitudinal radii, due to its $\cos^2(\theta)$ weighting in $Y_2^0$. The component $\Re C_2^2$ with its $\cos^2(\phi)$ weighting encodes the ratio between outward and sideward radii. Thus, the spherical harmonics method allows to obtain and analyze full three-dimensional femtoscopic information from a correlation function [25].

## 3.3 Experimental approach

The correlation function is defined as a probability to observe two particles together divided by the product of probabilities to observe each of them separately (Eq. 3.16). Experimentally this is achieved by dividing two distributions of relative momentum of pairs of particles coming from the same event and the equivalent distribution of pairs where each particle is taken from different collisions. In this way, one obtains not only femtoscopic information but also all other event-wide correlations. This method is useful for experimentalists to estimate the magnitude of non-femtoscopic effects. There exists also a different approach, where two particles in pairs in the second distribution are also taken from the same event. The second method gives only information about physical effects accessible via femtoscopy. The aim of this work is a study of effects coming from two particle interferometry, hence the latter method was used.

In order to calculate experimental correlation function, one uses the following approach. One has to construct two histograms: the *numerator* $N$ and the *denominator* $D$ with the particle pairs momenta, where particles are coming from the same event. Those histograms can be one-dimensional (as a function of $|\mathbf{q}|$), three dimensional (a function of three components of $\mathbf{q}$ in LCMS) or a set of one-dimensional histogram representing components of the spherical harmonic decomposition of the distribution. The second histogram, $D$ is filled for each pair with the weight 1.0 at a corresponding relative momentum $\mathbf{q} = 2\mathbf{k}^*$. The first one, $N$ is filled with the same procedure, but the weight is calculated as $|\Psi_{ab}(\mathbf{r}^*, \mathbf{k}^*)|^2$. A division $N/D$ gives the correlation function $C$. This procedure can be simply written as [25]:

$$C(\mathbf{k}^*) = \frac{N}{D} = \frac{\sum\limits_{n_i \in D} \delta(\mathbf{k}^*{}_i - \mathbf{k}^*)|\Psi_{ab}(\mathbf{r}^*{}_i, \mathbf{k}^*{}_i)|^2}{\sum\limits_{n_i \in D} \delta(\mathbf{k}^*{}_i - \mathbf{k}^*)} \,. \tag{3.25}$$

The $D$ histogram represents the set of all particle pairs used in calculations. The $n_i$ is a pair with the its relative momentum $\mathbf{k}^*{}_i$ and relative separation $\mathbf{r}^*{}_i$. The wave function used in Eq. 3.25 has one of the following forms:

$$|\Psi_{\pi\pi}(\mathbf{r}^*, \mathbf{k}^*)|^2 = |\Psi_{KK}(\mathbf{r}^*, \mathbf{k}^*)|^2 = 1 + \cos(2\mathbf{k}^*\mathbf{r}^*) \,, \tag{3.26}$$

$$|\Psi_{pp}(\mathbf{r}^*, \mathbf{k}^*)|^2 = 1 - \frac{1}{2}\cos(2\mathbf{k}^*\mathbf{r}^*) \,. \tag{3.27}$$

The first one is used in case of bosons, and the latter one is for identical fermions. Mathematically, the procedure of calculating the Eq. 3.25 is equivalent to a calculation of an integral in Eq. 3.17 through a Monte-Carlo method.

## 3.4 Scaling of femtoscopic radii

In the hydrodynamic models describing expansion of a quark-gluon plasma, particles are emitted from the source elements. Each of the source elements is moving with the velocity $u_\mu$ given by hydrodynamic equations. Because solutions of those equations are smooth, nearby source elements have similar velocities. Each emitted particle from a certain source element is boosted with the flow velocity $u_\mu$ according to the point of origin. Hence particles emitted close to each other (pairs with large transverse momentum $|\mathbf{k}_T|$) will gain the similar velocity boost, they can combine into pairs with small relative momenta ($|\mathbf{q}|$) and therefore become correlated. If the two particles are emitted far away from each other (a pair with small $|\mathbf{k}_T|$), the flow field $u_\mu$ in their point of emission might be very different and it will be impossible for them to have sufficiently small relative momenta in order to be in region of interference effect. This effect is visible in a width of a correlation function in the Fig. 3.4. The correlation function gets broader for greater values of $|\mathbf{k}_T|$ and the femtoscopic radius $R$ becomes smaller [8, 27].

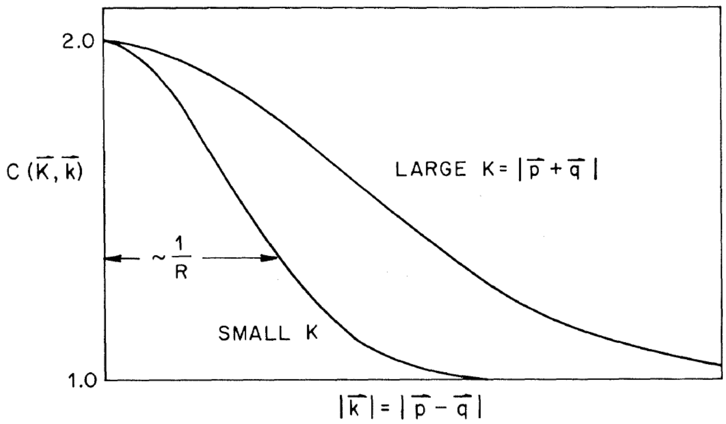


Figure 3.4: Correlation function width dependence on total pair momentum. Pion pairs with a large total momentum are more correlated [27].

### 3.4.1 Scaling in LCMS

Hydrodynamic calculations performed in LCMS show that femtoscopic radii in outward, sideward, and longitudinal direction show dependence on $m_T = \sqrt{k_T^2 + m}$, where $m$ is a mass of a particle [28]. This dependence can be expressed as follows:

$$R_x = \alpha m_T^{-\beta} , \tag{3.28}$$

where $x$ subscript indicates that this equation applies to $R_{out}$, $R_{side}$ and $R_{long}$ radii. The $\beta$ exponent is approximately equal 0.5. In case of strong transversal expansion of the source, the decrease of longitudinal interferometry radius can be more quick than $m_T^{-0.5}$, hence one can expect for longitudinal radii lower values of $\beta < 0.5$ [28].

### 3.4.2 Scaling in PRF

# Chapter 4

# Results

## 4.1 Identical particles correlations

## 4.2 Results of the fit

## 4.3 Discussion of results

# Chapter 5

# Summary

# Bibliography


[1] Standard Model of Elementary Paticles - Wikipedia, the free encyclopedia `http://en.wikipedia.org/wiki/standard_model`.

[2] R. Aaij et al. (LHCb Collaboration). Observation of the resonant character of the $z(4430)^{-}$ state. *Phys. Rev. Lett.*, 112:222002, Jun 2014.

[3] Donald H. Perkins. *Introduction to High Energy Physics*. Cambridge University Press, fourth edition, 2000. Cambridge Books Online.

[4] G. Odyniec. *Phase Diagram of Quantum Chromo-Dynamics* - course at Faculty of Physics, Warsaw University of Technology, Jun 2012.

[5] J. Beringer et al. (Particle Data Group). The Review of Particle Physics. *Phys. Rev.*, D86:010001, 2012.

[6] Z. Fodor and S.D. Katz. The Phase diagram of quantum chromodynamics. 2009.

[7] F. Karsch. Lattice results on QCD thermodynamics. *Nuclear Physics A*, 698(1-4):199 – 208, 2002.

[8] Adam Kisiel. *Studies of non-identical meson-meson correlations at low relative velocities in relativistic heavy-ion collisions registered in the STAR experiment*. PhD thesis, Warsaw University of Technology, Aug 2004.

[9] J. Bartke. *Relativistic Heavy Ion Physics*. World Scientific Pub., 2009.

[10] W. Florkowski. *Phenomenology of Ultra-Relativistic Heavy-Ion Collisions*. World Scientific, 2010.

[11] Science Grid This Week, October 25, 2006 - Probing the Perfect Liquid with the STAR Grid `http://www.interactions.org/sgtw/2006/1025/star_grid_more.html`.

[12] K. Grebieszkow. Fizyka zderzeń ciężkich jonów, `http://www.if.pw.edu.pl/~kperl/hip/hip.html`.

[13] Ulrich W. Heinz. From SPS to RHIC: Maurice and the CERN heavy-ion programme. *Phys.Scripta*, 78:028005, 2008.

[14] J. Adams et al. Identified particle distributions in pp and Au+Au collisions at s(NN)**(1/2) = 200 GeV. *Phys.Rev.Lett.*, 92:112301, 2004.

[15] G. David, R. Rapp, and Z. Xu. Electromagnetic Probes at RHIC-II. *Phys.Rept.*, 462:176–217, 2008.

[16] A. Marin et al. Dilepton measurements with CERES. *PoS*, CPOD07:034, 2007.

[17] John Adams et al. Experimental and theoretical challenges in the search for the quark gluon plasma: The STAR Collaboration's critical assessment of the evidence from RHIC collisions. *Nucl.Phys.*, A757:102–183, 2005.

[18] Adam Kisiel, Tomasz Taluc, Wojciech Broniowski, and Wojciech Florkowski. THERMINATOR: THERMal heavy-IoN generATOR. *Comput.Phys.Commun.*, 174:669–687, 2006.

[19] Mikolaj Chojnacki, Adam Kisiel, Wojciech Florkowski, and Wojciech Broniowski. THERMINATOR 2: THERMal heavy IoN generATOR 2. *Comput.Phys.Commun.*, 183:746–773, 2012.

[20] I. et al (BRAHMS Collaboration) Bearden. Charged meson rapidity distributions in central $\mathrm{Au} + \mathrm{Au}$ collisions at $\sqrt{s_{NN}} = 200\ \mathrm{GeV}$. *Phys. Rev. Lett.*, 94:162301, Apr 2005.

[21] W. Israel and J.M. Stewart. Transient relativistic thermodynamics and kinetic theory. *Annals of Physics*, 118(2):341 – 372, 1979.

[22] Piotr Bożek. Flow and interferometry in (3 + 1)-dimensional viscous hydrodynamics. *Phys. Rev. C*, 85:034901, Mar 2012.

[23] K. Kovtun, P. D. T. Son, and A. O. Starinets. Viscosity in strongly interacting quantum field theories from black hole physics. *Phys. Rev. Lett.*, 94:111601, Mar 2005.

[24] Fred Cooper and Graham Frye. Single-particle distribution in the hydrodynamic and statistical thermodynamic models of multiparticle production. *Phys. Rev. D*, 10:186–189, Jul 1974.

[25] Adam Kisiel. Nonidentical-particle femtoscopy at $\sqrt{s_{NN}} = 200$ GeV in hydrodynamics with statistical hadronization. *Phys. Rev. C*, 81:064906, Jun 2010.

[26] Adam Kisiel and David A. Brown. Efficient and robust calculation of femtoscopic correlation functions in spherical harmonics directly from the raw pairs measured in heavy-ion collisions. *Phys.Rev.*, C80:064911, 2009.

[27] S. Pratt. Pion Interferometry for Exploding Sources. *Phys.Rev.Lett.*, 53:1219–1221, 1984.

[28] S.V. Akkelin and Yu.M. Sinyukov. The HBT-interferometry of expanding inhomogeneous sources. *Z.Phys.*, C72:501–507, 1996.

# List of Figures